Foam-assisted chemical flooding for enhanced oil recovery
Effects of slug salinity and drive foam strength

Janssen, Martijn T.G.; Mutawa, Abdulaziz S.; Pilus, Rashidah M.; Zitha, Pacelli L.J.

DOI
10.1021/acs.energyfuels.9b00645

Publication date
2019

Document Version
Final published version

Published in
Energy and Fuels

energy&fuels

Article

Cite This: Energy Fuels 2019, 33, 4951−4963

pubs.acs.org/EF

Foam-Assisted Chemical Flooding for Enhanced Oil Recovery: Effects of Slug Salinity and Drive Foam Strength

Martijn T. G. Janssen,*[,†] Abdulaziz S. Mutawa,[†] Rashidah M. Pilus,[‡] and Pacelli L. J. Zitha[†]

[†]Petroleum Engineering Department, Delft University of Technology, 2628 CN Delft, The Netherlands

[‡]Petroleum Engineering Department, University Teknologi Petronas, 32610 Seri Iskander, Perak, Malaysia

Supporting Information

ABSTRACT: The novel enhanced oil recovery (EOR) technique combining the reduction of oil/water (o/w) interfacial tensions (IFT) to ultralow values and generation of a foam drive for mobility control is known as foam-assisted chemical flooding (FACF). We present a well-controlled laboratory study on the feasibility of FACF at reservoir conditions. Two specially selected chemical surfactants were screened on their stability in sea water at 90 °C. The ability of both surfactants to generate stable foam in bulk was studied in the presence and absence of crude oil. It led to the composition of the foam drive formulation for drive mobility control. Phase behavior scan studies, for the two crude oil/surfactant/brine systems, yielded the design of the chemical slug capable of mobilizing residual oil by drastically lowering the o/w IFT. Core-flood experiments were performed in Bentheimer sandstones previously brought to a residual oil to waterflood of 0.33 ± 0.02. A surfactant slug at under-optimum (o/w IFT of 10^{-2} mN/m) or optimum (o/w IFT of 10^{-3} mN/m) salinity was injected for mobilizing residual oil. It resulted in the formation of an unstable oil bank because of dominant gravitational forces at both salinities. Next, a foam drive was generated either in situ, by co-injecting nitrogen gas and surfactant solution, or pregenerated ex situ and then injected to displace the oil bank. We found that (i) the presence of the crude oil used in this work has a detrimental effect on foam stability in bulk and foam strength in Bentheimer sandstones, (ii) optimum salinity FACF was able to increase the ultimate oil recovery with 5% of the oil in place (OIP) after water flooding compared with under-optimum FACF, and (iii) injection of pregenerated drive foam increased its ultimate oil recovery by 13% of the OIP after water flooding compared to in situ drive foam generation at optimum salinity.

1. INTRODUCTION

Gas injection is a common and widely applied method for enhanced oil recovery (EOR). However, because of high gas mobility, recovery factors obtained during gas injection are often lower than anticipated as gas tends to override the water and oil in place (OIP). Moreover, viscous fingering and gas channeling through high-permeability streaks in the porous medium further magnifies its poor volumetric sweep efficiency.[1−3] Water-alternating-gas (WAG) injection, that is, the injection of gas slugs alternated by slugs of water, has been successfully applied for partially overcoming the drawbacks of continuous gas injection.[4−6] Nonetheless, gravity segregation might also occur during WAG flooding, yielding again an early breakthrough of gas.[7] Another approach to reduce gas mobility and hence increase its volumetric sweep efficiency is foaming of the gas. Foam involves a discontinuous gas phase, that is, gas bubbles, within a continuous liquid phase.[8−13] Foam stability is a strong function of the lamellae thickness, that is, thin aqueous films that separate gas bubbles within the foam texture, where thinner lamellae tend to rupture more easily.[14,15] The formation of foam is facilitated through the addition of a foaming agent, for example, a surfactant, to the aqueous phase that inhibits coalescence of separated gas bubbles thus promoting foam stability.

Besides a favorable volumetric sweep efficiency, the displacement efficiency, that is, fraction of oil mobilized in the swept region, needs to be sufficiently large as well in order to have a successful chemical EOR process. In previously extensive waterflooded reservoirs with good pore connectivity, residual oil remain trapped in the pore network, in the form of disconnected clusters and/or oil fragments,[16,17] because of the dominance of capillary forces. Moreover, if the rock surface is mixed- or oil-wet, oil might be adsorbed on the rock. Part of the trapped residual oleic phase may be mobilized through the injection of specially designed surfactants by a combined effect of rock wettability alteration toward more water-wet conditions[18,19] (mixed- or oil-wet reservoirs) and the reduction of the oil/water (o/w) interfacial tension (IFT) to ultralow values.[6,20−23] By altering the contact angle (θ), that is, the angle between rock and o/w interface, from oil-wet ($\theta > 90°$) conditions toward a water-wet ($\theta < 90°$) system, the surfactants may promote a rock that has a stronger attraction toward brine than oil, which might favor oil mobilization. In this case, the resulting capillary pressure yields water to imbibe more easily, compared to the oil-wet conditions.[24−26] A significant reduction of the o/w IFT would directly lead to a lower capillary pressure which increases the ratio of viscous forces over capillary forces that promotes oil mobilization.[14] To which extent a constant surfactant concentration can lower the o/w IFT is mainly controlled by the aqueous phase salinity.[27] An oil-in-water micro-emulsion (ME) is in equilibrium with excess oil (type II− system) at under-

Received: March 4, 2019
Revised: April 24, 2019
Published: April 29, 2019

optimum salinity conditions, whereas at over-optimum salinity a water-in-oil ME co-exists with excess water (type II+ system). In between the type II− and type II+ systems, an optimum salinity range can be identified (type III system) where a distinct ME is in equilibrium with excess oil and water. The type III system reveals ultralow o/w IFTs.

Recently, we have studied the EOR method of alkaline/surfactant/foam (ASF) flooding. ASF is based on the injection of an AS slug for the mobilization of residual oil followed by the generation of a drive foam (F) for mobility control.[6,21,23,28] Although the alkali might generate natural surfactants from the crude oil's naphthenic acids through a saponification process, in terms of practical aspects, the addition of alkali to the formulation may lead to internal corrosion of metal-based surface facilities (e.g., pipelines) because of the formation of carbonic acid.[29,30] The latter was our drive to come up with a chemical EOR methodology equivalent to ASF without the addition of alkali to the surfactant slug: Foam-assisted chemical flooding (FACF). Similar to ASF, FACF implies the injection of a surfactant slug at residual oil to waterflood for oil mobilization followed by the injection of a foam drive for mobility control.

Previous studies have shown that ASF is a viable EOR process (Figure 1).[6,21−23,31] However, bulk of the existing literature essentially use observed pressure and effluent data,[22,31] or have the assistance of limited single-energy CT scanning,[21] to describe related oil mobilization and displacement processes within the porous medium. Although some studies did vary the type of surfactants[31] and slug salinity,[6,22] we are not aware of any ASF/FACF related study that assessed multiple ways of drive foam injection (that is, in situ generated vs pregenerated).

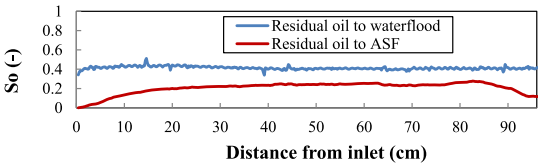

Figure 1. Residual oil saturation profiles obtained from core-flood experiments in a 1 m Bentheimer sandstone core: water flooding versus ASF.[6]

This work serves as a full extension of our earlier work on ASF at model-like conditions.[6,23] It reports on an elaborated laboratory study that addresses the feasibility of FACF to reservoir conditions instead of model-like settings. This study presents novel insights in terms of true dual-energy CT scan results that allowed us to study and visualize oil bank formation and its displacement by a foam drive on the core-scale, for varying slug salinity and the method of drive foam injection. The study includes surfactant stability, crude oil/surfactant phase behavior, and drive foam stability in bulk tests that yielded various surfactant formulations to be used in the ensuing core floods. Core-flood experiments include a foam quality scan, where one surfactant drive formulation was used to generate foam at varying gas fractional flows in the absence of oil, and a series of CT-scanned FACF experiments performed in Bentheimer sandstones. The assistance of a CT scanner with true dual-energy scanning capabilities allowed for novel qualitative and quantitative analysis of the oil bank formation and its displacement during FACF. The effects of surfactant slug salinity and drive foam strength on the FACF efficiency were studied by conducting FACF both at under-optimum and at optimum salinity conditions and comparing in situ drive foam generation through co-injection with the injection of pregenerated drive foam.

2. EXPERIMENTAL SECTION

2.1. Chemicals. In order to induce oil mobilization (by o/w IFT lowering) and gas foaming (achieving mobility control), two surfactants were selected: IOS2024 and a proprietary surfactant which will be designated as Surfactant X. IOS2024 is an anionic surfactant, while Surfactant X contains both anionic and amphoteric surfactants, the latter carrying simultaneously anionic and cationic hydrophilic groups. Both surfactants were found to be unstable in the vicinity of injection water, that is, sea water, at 90 °C as the magnesium (Mg^{2+}) and calcium (Ca^{2+}) ions present yield complexation and, finally, precipitation of both surfactants. It was decided to remove corresponding salts (magnesium chloride hexahydrate, $MgCl_2{\cdot}6H_2O$, and calcium chloride dehydrate, $CaCl_2{\cdot}2H_2O$) from the injection water composition and to compensate for its removal through the addition of sodium chloride (NaCl) equal in total ionic strength. The modified injection water formulation forms the basis for all aqueous solutions used throughout the entire study (Table S·I.2, see Supporting Information).

An overview of the physical properties of the chemicals used in this study is presented in Table S·I.1 (see Supporting Information). Brine was prepared by dissolving sodium chloride, sodium sulphate, potassium chloride, and sodium bicarbonate in demineralized water. Surfactant slug solutions were prepared by adding required amounts of surfactant and 2-butanol, a cosolvent, to brine. The cosolvent was added to the surfactant slug formulation to guarantee its stability.[20] Surfactant drive formulations were prepared by adding the necessary amounts of surfactant to brine. Nitrogen gas was used for co-injection with surfactant drive solution for in situ foam generation and for creating pregenerated drive foam. A crude oil was used in the core-flood experiments. Its acid and base numbers were measured and equaled 0.17 and 0.32 mg KOH/g, respectively. In two FACF core-flood experiments the oleic phase was doped with 20 weight percent (wt %) 1-iododecane for enhancement of the CT contrast between the oleic and aqueous phases. Aqueous solutions were degassed under vacuum prior to injection.

Table 1. Properties of the Bentheimer Sandstone Cores Used

	experiment				
parameter	1	2	3	4	5
porosity (%)	23.0 ± 0.1[b]	23.0 ± 0.1[b]	21.8 ± 0.3[a]	22.4 ± 0.4[a]	23.0 ± 0.1[b]
permeability (D)	3.42 ± 0.20	2.48 ± 0.50	3.58 ± 0.30	3.73 ± 0.30	3.76 ± 0.20
length (cm)	40.00 ± 0.10	40.00 ± 0.10	40.00 ± 0.10	40.00 ± 0.10	40.00 ± 0.10
diameter (cm)	3.80 ± 0.10	3.80 ± 0.10	3.80 ± 0.10	3.80 ± 0.10	3.80 ± 0.10
pore volume (cm^3)	104.34 ± 6.32	104.34 ± 6.32	98.89 ± 6.98	101.62 ± 7.60	104.34 ± 6.32

[a]Porosity values reported were calculated using obtained CT data. [b]Porosity values shown were obtained from a representative measurement using the Ultra Pycnometer 1000.

DOI: 10.1021/acs.energyfuels.9b00645
Energy Fuels 2019, 33, 4951−4963

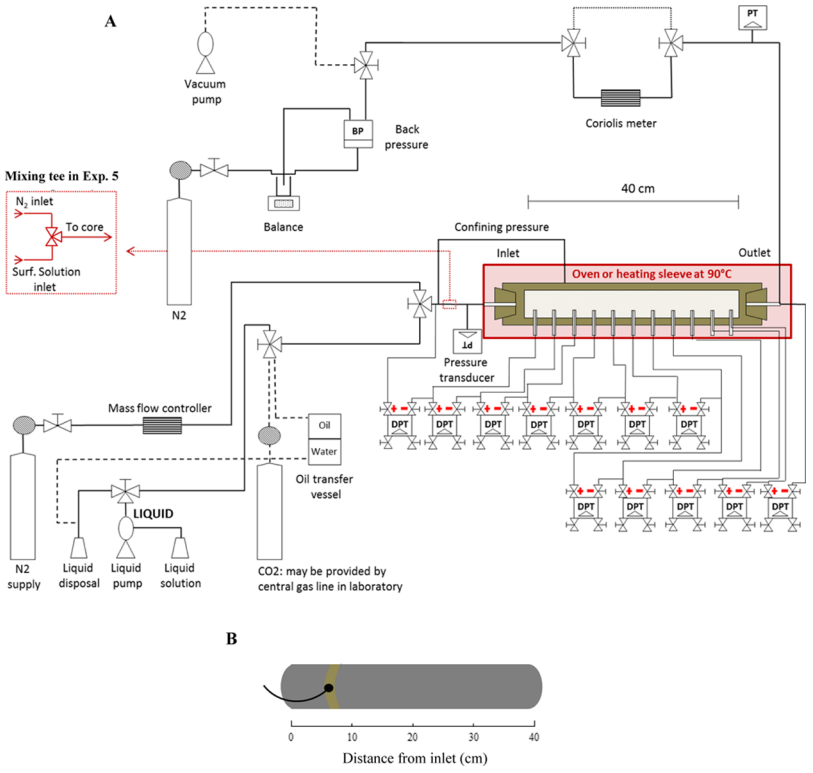

Figure 2. (A) schematic of experimental setup (B) for CT-assisted core-floods a heating sleeve (grey) was used instead of an oven. Because of the position of the inlet port of the confining pressure (black), two separate heating sleeves were used. It resulted in a small section (5.6−8.6 cm from inlet) of the core-holder (brown) being uncovered by the sleeves.

Table 2. Overview of Core-Flood Experiments Performed

exp.	process	salinity	foam quality (%)	liquid flow rate (cm^3/min)	gas flow rate (cm^3/min)	total injection velocity (ft/day)	CT	method of drive foam generation
1	foam quality scan		multiple	multiple	multiple	2.1 ± 0.1	no	co-injection
2	FACF	under-optimum	57.5	0.2125	0.2875	2.1 ± 0.1	no	co-injection
3	FACF	under-optimum	57.5	0.2125	0.2875	2.1 ± 0.1	yes	co-injection
4	FACF	optimum	57.5	0.2125	0.2875	2.1 ± 0.1	yes	co-injection
5	FACF	optimum	57.5	0.2125	0.2875	2.1 ± 0.1	no	pre-generated

2.2. Core Samples. Reservoir rocks for the studied oil field are exclusively sandstones that exhibit good reservoir characteristics in terms of porosity (up to 25%) and permeability (up to 640 mD). Bentheimer sandstone cores were used in this study to mimic reservoir rocks because of its homogeneous mineralogy (>91 wt % Quartz) and high permeabilities (3.39 ± 0.91 D).[32] Its physical properties are presented in Table 1. Porosities shown were either determined from CT scan data or by using an Ultra Pycnometer 1000 (Quantachrome Corporation). Several equidistant holes were drilled in the cores for pressure drop measurements. All cores were placed horizontally. More details about the preparation of the sandstone samples are given elsewhere.[6]

2.3. Equipment: Bulk Foam Experiments. Bulk foam stability experiments were performed using two surfactant formulations studied in this work: IOS2024 and Surfactant X. Experiments were conducted in the absence and presence of crude oil utilizing the Foam Scan instrument (I.T. Concept-TECLIS). The apparatus is designed to measure (i) the ability of a liquid to develop foam by sparging N_2 through it, and (ii) the stability of the generated foam by monitoring its volume as function of time.

2.4. Equipment: Core-Flood Experiments. Core-flood experiments were conducted utilizing the experimental setup shown in Figure 2. Bentheimer sandstone cores were placed horizontally in a designed core holder made of polyether ether ketone which exhibits low X-ray attenuation and high mechanical strength. The confining pressure, that is, the pressure in the core holder surrounding the sandstone, was set equal to the inlet pressure in all experiments performed. Aqueous solutions were injected using a dual-cylinder liquid pump (Quizix QX-6000), placed in line with the core-holder. A separate transfer vessel was used for injecting the crude oil. Several absolute and differential pressure transducers were installed along the core for accurately monitoring pressure (drop) behavior during the various injection stages. Thermocouples were connected to the setup for temperature monitoring. The (differential) pressure transducers and thermocouples were linked to a USB data acquisition system (National Instruments, cDAQ-9174) that recorded the data using a 5 s time interval. The outlet pressure was set using a backpressure regulator (DEMO-TU Delft). For regulating the N_2 fractional flow during drive foam injection, that is, foam quality, a mass flow controller (Bronkhorst, EL-FLOW) was used. A Coriolis flowmeter (Bronkhorst, CORI-FLOW), which measured effluent densities and mass flow rates, was connected to the outlet for accurately determining phase breakthrough times. Effluent fluids were collected in a measuring cup placed on a digital balance. CO_2, used for initial flushing of the core (Section 2.7), was supplied in a 200 bar cylinder. In one FACF core-flood, exp. 5 in Table 2, a high-pressure static mixing tee (Health & Science, U-466), which features a 10 μm stainless steel frit, was placed at the inlet section in order to pregenerate foam prior to injection. The frit pore size of 10 μm corresponds well with averaged pore body and throat diameters

DOI: 10.1021/acs.energyfuels.9b00645
Energy Fuels 2019, 33, 4951−4963

reported for Bentheimer sandstones.[32] All core-flood experiments were conducted at a reservoir temperature of 90 ± 1 °C. Temperature was either controlled by (i) placing the core holder in an oven (exp. 1, 2, and 5 in Table 2), or by (ii) utilizing aluminum heating sleeves filled with silicon oil for CT-assisted core-floods (exp. 3 and 4 in Table 2). Note that, because of the design of the core holder, two separate aluminum sleeves were used which led a short section of the core holder uncovered by the heating sleeves (Figure 2).

In exp. 3 and 4 (Table 2) a Siemens SOMATOM Definition CT scanner with true dual-energy scanning capabilities was utilized for quantifying three-phase saturation distributions during the various injection stages. It allowed for assessing and visualizing the oil bank formation and its displacement by a foam drive. A more detailed description of the apparatus is given elsewhere.[6]

2.5. Procedure: Phase Behavior. Phase behavior tests were conducted by preparing several crude oil/surfactant slug formulations where the surfactant slug contained *X* wt % NaCl, 0.37 wt % Na_2SO_4, *X*/53.3 wt % KCl, 0.03 wt % $NaHCO_3$, 1.00 wt % 2-butanol, and 0.30 wt % active matter (AM) IOS2024 or 0.30 wt % AM Surfactant X. Both NaCl and KCl concentrations were altered in order to vary slug salinity because we aimed to change solely the monovalent chloride ions. Crude oil/surfactant slug mixtures were prepared at a 1:2 oil-to-water ratio and subsequently placed on a shaking roller for 10 h to ensure adequate mixing. Afterward, the samples were placed in an oven at 90 °C until equilibrium was reached (typically after 3 weeks). The oil and water solubilization ratios were then estimated by assuming that all the surfactant is present in the ME phase and not in the excess oil or water phases.[14] Optimum salinity was determined as the salinity at which the oil and water solubilization ratios overlap. The goal of the phase behavior study is to identify the surfactant slug formulation (IOS2024 or Surfactant X) that will be used in the FACF core-floods and to categorize the Winsor type systems of the final surfactant slug composition.[27] All phase behavior tests were performed at ambient pressure and the core-floods were conducted using a backpressure of 20 bar. The potential pressure effect implies an increasing optimum salinity range (type III system) with increasing pressure.[33] However, this effect is expected to be insignificant when dealing with a pressure difference of only 20 bar.

2.6. Procedure: Bulk Foam. In order to assess drive foam stability in bulk for both IOS2024 and Surfactant X, bulk foam experiments were conducted in the absence of crude oil. The two surfactant drive solutions studied contained 3.44 wt % NaCl, 0.37 wt % Na_2SO_4, 0.06 wt % KCl, 0.03 wt % $NaHCO_3$, and 0.50 wt % AM IOS2024 or 0.50 wt % AM Surfactant X. Surfactant solutions (40.0 ± 0.5 cm^3) were placed in the sample holder. Then, N_2 was sparged into the surfactant solutions (at 20 cm^3/min) until the volume of the generated foam column reached 110 ± 1 cm^3. Next, N_2 gas supply was shut off and the foam volume was monitored over time. The bulk foam experiments were performed at 20 ± 1 °C and at atmospheric pressure. The goal of abovementioned tests is to select the surfactant drive solution that yielded the most stable foam in bulk; this drive formulation will be used in the succeeding FACF core-floods. Although core-flood experiments were conducted at 90 ± 1 °C, the anticipated temperature effect on foam stability in bulk (that is, earlier foam decay at higher temperatures because of reduction in liquid viscosity) is expected to be similar for both surfactant drive formulations.[34] The latter implies that comparing the results of the bulk foam tests performed at 20 ± 1 °C is still qualitatively valid for 90 ± 1 °C. Lastly, the impact of crude oil on the stability of the selected surfactant drive foam in bulk was studied by performing one additional bulk foam test. It included 5 volume percent (vol %) crude oil to the initial amount of liquid surfactant solution placed in the sample holder.

2.7. Procedure: Core-Floods. Table 2 gives an overview of the core-flood experiments performed in this study. The sequence used for performing all five core floods is presented in Table 3. After flushing the core with CO_2 and evacuated the system to −1 bar, to remove all the air inside the core, approximately 10.00 pore volume to liquid (PV) of brine were injected. During the last PV of brine injection, the backpressure was increased from atmospheric pressure to 25 bar to ensure complete dissolution of remaining CO_2 in brine. Next, in exp. 1, a surfactant drive preflush of approximately 10.00 PV was conducted in order to satisfy the surfactant adsorption capacity of the rock. Afterward, drive foam was generated at various gas fractional flows in exp. 1. This was done through co-injection of the selected surfactant drive formulation and N_2 at a constant superficial velocity of 2.1 ± 0.1 ft/day. Results obtained from exp. 1 give an overview of steady-state foam strengths as a function of drive foam quality in the absence of crude oil. For all other core-flood experiments, subsequent to brine injection, crude oil was injected (circa 5.00 PV) for establishing connate water saturation (S_{wc}). Afterward, the system was exposed to extensive water flooding (nearly 7.00 PV) in order to reach residual oil to waterflood (S_{or_WF}). At the end of brine injection, oil injection and water flooding, injection rates were varied for determining the absolute permeability to brine and the oil and water end-point relative permeabilities (k^*_{ro} and k^*_{rw}), respectively, by using Darcy's law.[35] Prior to changing injection rates for k^*_{ro} and k^*_{rw} estimation during primary drainage and water flooding, respectively, bump floods were applied by increasing the injection rate with a factor 8 (oil injection) or 16 (water flooding) in order to establish true initial oil saturation (S_{oi}) and S_{or_WF}. Next to water flooding, in exp. 2, 3, 4, and 5, approximately 0.45 PV of surfactant slug was injected at 0.6 ± 0.1 ft/day, at either under-optimum (exp. 2 and 3) or at optimum (exp. 4 and 5) salinity, in order to mobilize S_{or_WF}. Consequently, for displacing the formed oil bank, drive foam was generated either in situ through co-injection of N_2 and surfactant drive solution (exp. 2, 3, and 4) or by injecting pre-generated foam (exp. 5), all at a constant foam quality of 57.5% and a total superficial velocity of 2.1 ± 0.1 ft/day (Table 2). Drive foam injection continued until no more measurable amounts of oil were produced. Although exp. 5 was not conducted with the assistance of a medical CT scanner, still the oleic phase was doped with 1-iododecane in order to allow for comparison of the results with exp. 4. Table S.I.2 (Supporting Information) gives an overview of the physical properties of the various types of brine, oil, surfactant slug, and drive solutions utilized in this study. In order to avoid any brine-slug-drive salinity gradient, the total ionic strength of each aqueous solution within one experiment was kept constant. More detailed information on the CT data postprocessing is explained elsewhere.[6]

Table 3. Core-Flood Procedure

step	exp.	process	back pressure (bar)	pore volumes injected	flow rate (cm^3/min)
1	all	CO_2 flushing			
2	all	vacuuming			
3	all	brine saturation	25	10.00	0.25
4	1[b]	surfactant drive pre-flush	20	10.00	0.50
5	2, 3, 4, 5	oil injection	20	5.00	0.50
6	2, 3, 4, 5	water flooding[a]	20	7.00	0.25
7	2, 3, 4, 5	surfactant slug injection	20	0.45	0.15
8	1[b], 2, 3, 4	surfactant drive co-injection	20		liquid: 0.2125
					gas: 0.2875
9	5	pre-generated foam injection	20		liquid: 0.2125
					gas: 0.2875

[a]For water flooding, the same synthetic brine was used as for brine saturation in the respective experiment. [b]In exp. 1 foam flooding was assessed at fully surfactant drive solution saturated conditions using various foam qualities while maintaining a superficial velocity of 2.1 ± 0.1 ft/day.

DOI: 10.1021/acs.energyfuels.9b00645
Energy Fuels 2019, 33, 4951−4963

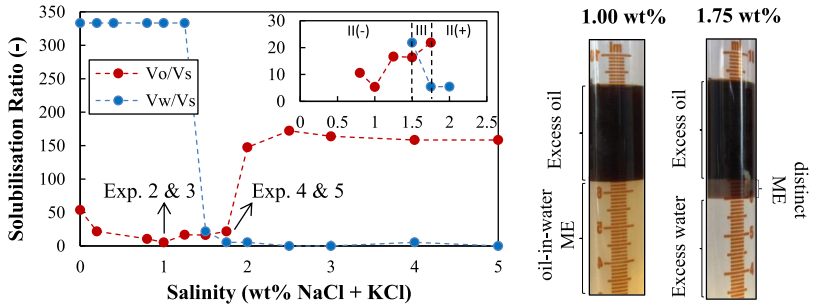

Figure 3. Solubilization ratios as function of salinity for the IOS2024 phase behavior study. Aqueous phase compositions consist of *X* wt % NaCl, 0.37 wt % Na_2SO_4, (*X*/53.3) wt % KCl, 0.03 wt % $NaHCO_3$, 1.00 wt % 2-butanol, and 0.30 wt % AM IOS2024. The top right diagram covers the optimum salinity range (type III system) which is found in between 1.50 and 1.75 wt % NaCl + KCl, the under-optimum range, type II(−) system (<1.50 wt % NaCl + KCl) and the over-optimum salinity conditions, type II(+) system (>1.75 wt % NaCl + KCl). Experiments 2 and 3 were performed at under-optimum salinity, whereas experiments 4 and 5 were performed at optimum salinity conditions. The right-hand side presents the two crude oil/surfactant slug mixtures, after being placed in an oven at 90 °C for three weeks, representative for the experimental conditions. Note the presence of a clear, distinct, ME at optimum salinity.

3. RESULTS AND DISCUSSION

3.1. Phase Behavior and Bulk Foam. The phase behavior study for the crude oil-Surfactant X system did not reveal a distinct ME phase for the entire range of salinities investigated (0.0−5.0 wt % NaCl + KCl). It showed that Surfactant X was not able to reduce the o/w IFT to ultra-low values. Hence, the discussion of the salinity scan will be restricted to the crude oil-IOS2024 system. Note that, unless otherwise stated, salinities refer to wt % NaCl + KCl. Figure 3 presents the oil and water solubilization ratios (V_o/V_s and V_w/V_s, respectively) as function of salinity for the crude oil-IOS2024 phase behavior study. The Winsor type III system, characterized by a distinct ME phase in equilibrium with clean excess oil and water, was found at salinities ranging from 1.50 to 1.75 wt %. The oil/ME (o/m) and water/ME (w/m) IFTs at these optimum salinities were estimated using Huh's empirical correlation and varied from 6.0×10^{-4} to 1.0×10^{-2} mN/m, respectively.[36] The under-optimum salinity regime, that is, Winsor type II− system, was observed for salinities below 1.50 wt %, whereas a Winsor type II+ system, that is, over-optimum regime, was found at salinities larger than 1.75 wt %. Exp. 2 and 3 were conducted at an under-optimum salinity of 1.00 wt %, whereas exp. 4 and 5 were done at an optimum salinity of 1.75 wt % (Figure 3 and Table S.I.2). The addition of 20 wt % 1-iododecane to the crude oil did not alter the phase behavior.

The foam half-decay times ($t_{1/2}$), that is, the time that it takes for the initial foam volume to be reduced by 50%, obtained in the three bulk foam experiments are shown in Table 4. The data show that Surfactant X was able to produce a much more stable drive foam in bulk ($t_{1/2}$ = 738 min) compared to IOS2024 ($t_{1/2}$ = 69 min), in the absence of crude oil. This resulted in Surfactant X to be selected for the drive foam formulation in succeeding FACF core-floods. To assess the impact of crude oil on bulk foam stabilized by Surfactant X, one additional test was conducted in the presence of 5 vol % crude oil. The presence of 5 vol % crude oil was able to reduce the $t_{1/2}$ of Surfactant X drive foam from 738 to 62 min, that is, a factor 12 reduction.

3.2. Foam Quality Scan. In exp. 1, a Surfactant X drive (see formulation in Table S.I.2) was co-injected with N_2 at varying foam qualities, that is, gas fractional flows, into a Bentheimer sandstone core (Table 1). The total, that is, gas + liquid, injection rate was kept constant at 2.1 ± 0.1 ft/day.

Table 4. Foam Half-Decay Times ($t_{1/2}$) Obtained during the Bulk Foam Experiments[a]

drive type	crude oil added (vol %)	$t_{1/2}$ (min)
3.44 wt % NaCl	0.0	69
0.37 wt % Na_2SO_4		
0.06 wt % KCl		
0.03 wt % $NaHCO_3$		
0.50 wt % AM IOS2024		
3.44 wt % NaCl	0.0	738
0.37 wt % Na_2SO_4		
0.06 wt % KCl		
0.03 wt % $NaHCO_3$		
0.50 wt % AM surfactant X		
3.44 wt % NaCl	5.0	62
0.37 wt % Na_2SO_4		
0.06 wt % KCl		
0.03 wt % $NaHCO_3$		
0.50 wt % AM surfactant X		

[a]All tests were conducted at 20 ± 1 °C and atmospheric pressure.

Measured steady-state pressure drops over the entire core length, for each single foam quality (f_g) studied, were used to estimate corresponding apparent foam viscosities (μ_{app} in Pa·s) by

$$\mu_{app} = \frac{k\nabla P}{(u_l + u_g)} \quad (1)$$

where k, u_l, u_g, and ∇P represent the absolute permeability (m^2), liquid and gas superficial velocities (m/s) and the pressure gradient across the entire core (Pa/m), respectively. Corresponding foam apparent viscosities as function of foam quality are shown in Figure 4. Foam apparent viscosity increases with increasing foam quality from 0.63 ± 0.11 Pa·s at f_g = 20.0% to a maximum of 1.45 ± 0.11 Pa·s obtained at a critical foam quality (f_g^*) of 75.0%. For $f_g > f_g^*$, apparent viscosities slightly decrease to roughly 0.84 ± 0.08 Pa·s at f_g = 98.0%. The observed trend is consistent with data reported by others for similar foam systems.[37−39] Foam flow in the low-quality regime ($f_g < f_g^*$) is mainly affected by bubble trapping and the foam apparent viscosity is essentially controlled by the gas flow rate; increasing μ_{app} with increasing f_g. However, in the high-quality regime ($f_g > f_g^*$), foam behavior is influenced by bubble coalescence and here the foam apparent viscosity is

DOI: 10.1021/acs.energyfuels.9b00645
Energy Fuels 2019, 33, 4951−4963

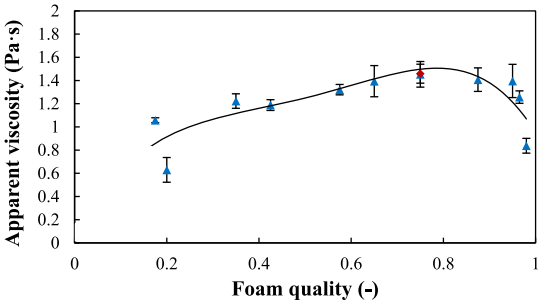

Figure 4. Apparent foam viscosity as function of foam quality at 90 ± 1 °C and 20 bar backpressure for the drive solution shown in Table S.I.2. For each foam quality investigated, co-injection continued until a steady-state pressure drop was observed. Foam flooding at f_g = 0.75 was repeated at the end of the experiment in order to verify its reproducibility (red diamond). A polynomial of the 4th order has been fitted to the data.

mostly dependent on the liquid superficial velocity; decreasing μ_{app} with increasing f_g. The Surfactant X drive formulation (Table S.I.2) proved to be able to generate strong, stable drive foams for the entire range of foam qualities studied in the absence of crude oil. Because previous studies have shown that high-quality foams are more vulnerable to the presence of oil than low-quality foams, the drive foam quality to be used in the following FACF core-floods (exp. 2, 3, 4, and 5) needs to be sufficiently lower than f_g^*.[40,41] It is for this reason that a fixed drive foam quality of 57.5% was used in all succeeding FACF core-flood experiments. The apparent foam viscosity of f_g = 57.5% equaled 1.32 ± 0.05 Pa·s.

Exp. 1 revealed that the Surfactant X drive solution (Table S.I.2) is capable of generating strong foams, over a wide range of foam qualities, in the absence of crude oil. In order to assess the effect of the crude oil on foam strength and stability in Bentheimer sandstone cores, N_2 and the same Surfactant X drive solution were co-injected (f_g = 57.5%) at S_{or_WF} = 0.34 ± 0.02 to generate foam. Results indicated a reduction in μ_{app} with roughly a factor of 170 compared to steady-state foam flow in the absence of crude oil: 0.007 ± 0.002 Pa·s. These observations, together with the bulk foam results discussed in Section 3.1, suggest that the crude oil is detrimental to foam strength and stability in both bulk and porous media. The composition of the crude oil (roughly 75 wt % consist of carbon chains from C1 to C12) might explain the detrimental impact as previously studied showed an increasing detrimental effect to foam stability, that is, increase of gas bubble coalescence, with reducing carbon chain lengths.[42,43] Whether the same observations are expected when applying Surfactant X drive foam in a FACF process is debatable as part of S_{or_WF} will be mobilized by injecting an IOS2024 surfactant slug prior to drive foam injection, lowering S_o, which might promote foaming.

3.3. FACF. Table 5 presents a summary of the performed FACF core-flood experiments (exp. 2, 3, 4, and 5). This section discusses the chemical EOR injection stages for all four experiments, that is, surfactant slug and surfactant drive foam injection. Results will be interpreted and discussed in terms of total pressure drops, oil saturation profiles, and ultimate oil recoveries. The preparatory injection stages, that is, primary drainage (oil injection) and forced imbibition (water flooding), are not discussed in detail here as they yield major similarities with our earlier work at model-like conditions.[6,23] The

Table 5. : Summary of FACF Core-Flood Experiments Performed. k_{ro}^*, k_{rw}^*, M, S_{wc}, S_{oi}, S_{or_WF}, S_{or_FACF}, R_{FWF}, R_{FFACF}, OIP, and OIIP Represent the Oil End-Point Relative Permeability, Water End-Point Relative Permeability, End-Point Mobility Ratio, Connate Water Saturation, Initial Oil Saturation, Residual Oil Saturation to Waterflood, Residual Oil Saturation to FACF, Recovery Factor Corresponding to Water Flooding, Recovery Factor Corresponding to FACF, Oil in Place, and the Oil Initially in Place, Respectively[a]

exp.	k_{ro}^*	k_{rw}^*	M	S_{wc}	S_{oi}	S_{or_WF}	S_{or_FACF}	R_{FWF} (% of OIIP)	R_{FFACF} (% of OIIP)	R_{FFACF} (% of OIP after WF)
2	0.54 ± 0.09	0.15 ± 0.02	0.75 ± 0.46	0.21 ± 0.02[b]	0.79 ± 0.02[b]	0.36 ± 0.01[b]	0.23 ± 0.01[b]	54 ± 3[b]	71 ± 2[b]	36 ± 5[b]
3	0.48 ± 0.03	0.20 ± 0.01	1.12 ± 0.37	0.25 ± 0.02[b]	0.75 ± 0.02[b]	0.31 ± 0.02[b]	0.20 ± 0.01[b]	59 ± 4[b]	73 ± 2[b]	35 ± 7[b]
				0.16 ± 0.08[c]	0.84 ± 0.08[c]	0.33 ± 0.02[c]	0.21 ± 0.03[c]	61 ± 5[c]	75 ± 5[c]	36 ± 13[c]
4	0.46 ± 0.03	0.22 ± 0.01	1.32 ± 0.38	0.23 ± 0.02[b]	0.77 ± 0.02[b]	0.30 ± 0.01[b]	0.18 ± 0.01[b]	61 ± 3[b]	77 ± 2[b]	40 ± 5[b]
				0.20 ± 0.09[c]	0.80 ± 0.09[c]	0.31 ± 0.05[c]	0.16 ± 0.06[c]	61 ± 10[c]	80 ± 9[c]	48 ± 24[c]
5	0.50 ± 0.03	0.15 ± 0.01	0.83 ± 0.26	0.20 ± 0.02[b]	0.80 ± 0.02[b]	0.34 ± 0.02[b]	0.16 ± 0.01[b]	58 ± 3[b]	80 ± 2[b]	53 ± 5[b]

[a]The end-point mobility ratios (M) were calculated using the following formula: $(k_{rw}^*/\mu_w)/(k_{ro}^*/\mu_o)$ where μ_w and μ_o represent the water and oil viscosity at 90 °C, respectively. R_{FFACF} as a function of OIP after WF is calculated in exp. 3 and 4 based on CT processing as follows: $((S_{or\_WF} - S_{or\_FACF})/S_{or\_WF}) \times 100$. Corresponding relatively large error is mainly due to the nonuniform distribution of S_{or_FACF}, which is of a higher magnitude in exp. 4 compared to exp. 3. The fairly large error in S_{wc} and S_{oi} obtained from CT processing in exp. 3 and 4, is due to the presence of the capillary end effect.[23] [b]Based on material balance calculations. [c]Based on CT processing.

DOI: 10.1021/acs.energyfuels.9b00645
Energy Fuels 2019, 33, 4951−4963

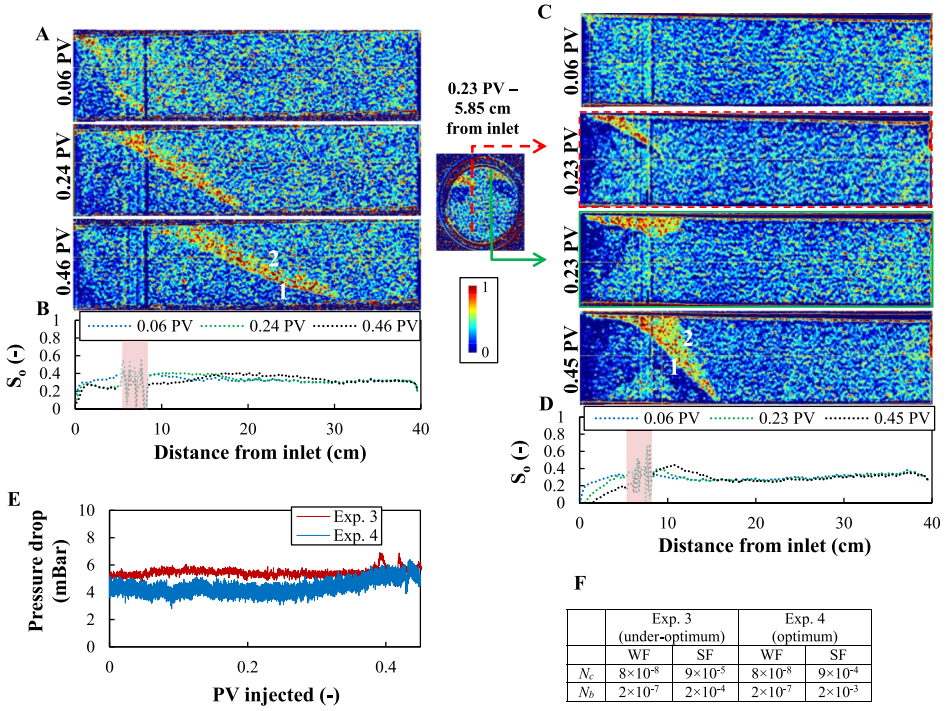

	Exp. 3 (under-optimum)		Exp. 4 (optimum)	
	WF	SF	WF	SF
N_c	8×10^{-8}	9×10^{-5}	8×10^{-8}	9×10^{-4}
N_b	2×10^{-7}	2×10^{-4}	2×10^{-7}	2×10^{-3}

Figure 5. Two-dimensional CT images taken during surfactant slug injection at under-optimum salinity, exp. 3 (A), and during slug injection at optimum salinity, exp. 4 (C) and related S_o profiles (B,D). CT images shown were taken at the center of the core by default. At 0.23 PV injection at optimum slug salinity two cross-sections are shown, both deviating from the center of the core, because of heterogeneous characteristics of the oil bank's shape at that injection time. Numbers 1 and 2 refer to the two displacement interfaces present at the upstream and downstream side of the oil bank, respectively. The edges of the two heating sleeves used (Figure 2B) resulted in CT artifacts of a significant magnitude in between 5.6 and 8.6 cm distance from the inlet (red band in graphs B,D). Note that for further CT analysis these areas were ignored. The bottom left graph (E) presents the total pressure drop values obtained during surfactant slug injection for both exp. 3 and 4. Table F shows the related capillary numbers (N_c) and bond numbers (N_b) during water flooding (WF) and surfactant slug injection (SF) for both experiments. Capillary numbers were calculated using $N_c = (\mu^* u)/\sigma$ where μ, u and σ represent the fluid viscosity, injection velocity, and the o/w IFT, respectively. Bond numbers were estimated using $N_b = (\Delta\rho^* g^* K)/\sigma$ where $\Delta\rho$, g, and K represent the density difference, gravitational constant, and absolute permeability, respectively.

variation in the end-point mobility ratio (M), representative for oil displacement during water flooding, is mainly because of differences in k^*_{ro} and k^*_{rw} (Table 5). The more water-wet the system is, the larger is the difference between k^*_{ro} and k^*_{rw}, the lower M.

3.3.1. Mobilizing S_{or_WF} at under-Optimum and Optimum Slug Salinity. After reaching S_{or_WF} in exp. 2 to 5 (Table 5), an IOS2024-based surfactant slug (Table S.I.2) was injected, either at under-optimum (exp. 2 and 3) or at optimum (exp. 4 and 5) salinity conditions, for promoting oil mobilization by reducing the capillary forces that kept S_{or_WF} in place. The analysis in this section will be limited to exp. 3 and 4 only because both were performed with the assistance of a medical CT scanner and the other FACF core-floods showed similar results in terms of observed pressure drops.

Total pressure drops, CT scan images, and related S_o profiles during surfactant slug injection in exp. 3 and 4 are presented in Figure 5. At first, CT images and associated S_o profiles will be discussed as they give insight in saturation distributions which affect measured total pressure drops. The images for exp. 3 (Figure 5A) indicate that injection of the under-optimum surfactant slug-mobilized part of S_{or_WF} rather efficiently, leading to the formation of an oil bank. The tilted oil bank shape is a consequence of the difference in propagation velocity between its leading edge (53 ± 2 cm/PV), that is, downstream side, and its trailing edge (29 ± 1 cm/PV), that is, its upstream side. The driving force for the latter is the effective density difference between the injected surfactant slug and the oil and water in place ($\Delta\rho$ = 0.047 ± 0.003 g/cm^3), which resulted in a gravity underriding tongue of the injected slug. It is expected that at the pore scale the gravity effect is substantially reduced because of a significant reduction in length scale. The under-optimum slug proved to be able to reduce S_{or_WF} by roughly 30% upstream of the oil bank after 0.46 PV injection, yielding an average S_o of 0.23 ± 0.05 in that section. The averaged peak S_o in the oil bank remained fairly constant over time and equaled 0.41 ± 0.01 at the end of slug injection.

The CT images for surfactant slug injection at optimum salinity (exp. 4) show, similar to under-optimum salinity injection, the formation of an unstable, diffuse, oil bank (Figure 5C). However, some distinctive features can be observed. One of them is the magnitude of oil mobilization by the injected slug. At optimum salinity, the slug was significantly more effective at mobilizing S_{or_WF}, yielding an average S_o of 0.06 ± 0.06 (81% reduction of S_{or_WF}) at the end of slug injection upstream of the oil bank's trailing edge. It can be attributed to the increase in capillary number from 10^{-5} (under-optimum salinity) to 10^{-4} (optimum salinity) due to the change in o/w IFT from 10^{-2} to 10^{-3} mN/m upon switching from under-optimum to optimum salinity conditions. Furthermore, peak S_o tends to increase as function of injection time, yielding a somewhat higher peak S_o (0.45 ± 0.01) in the oil bank at the end of slug injection compared to exp. 3. At 0.23 PV of

DOI: 10.1021/acs.energyfuels.9b00645
Energy Fuels 2019, 33, 4951−4963

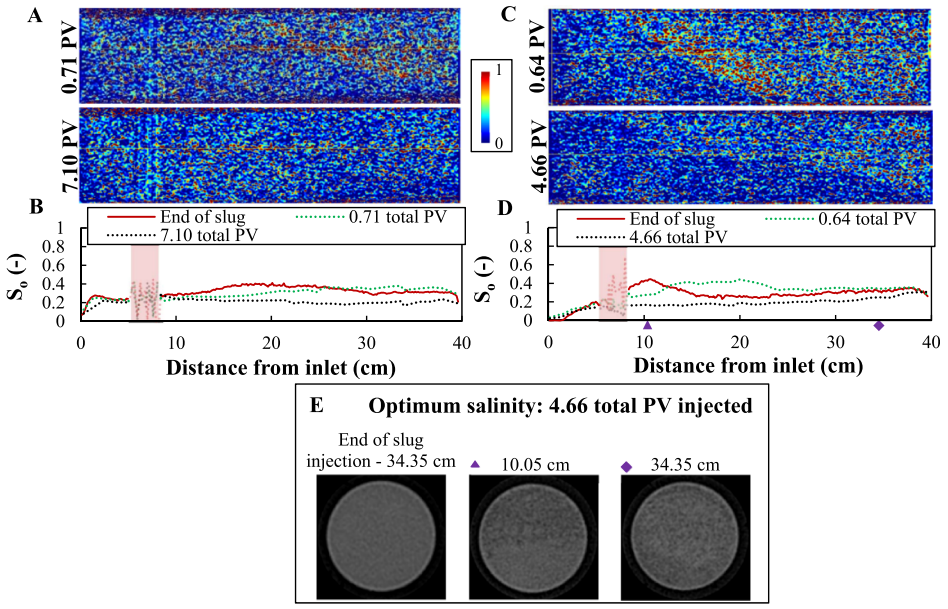

Figure 6. CT images taken during drive co-injection at under-optimum salinity, exp. 3 (A), and at optimum salinity, exp. 4 (C) and related oil saturation profiles (B,D). CT images shown were taken at the center of the core. Total PV = 0 refers to the start of surfactant slug injection. The edges of the two heating sleeves used (Figure 2B) resulted in CT artifacts of a significant magnitude in between 5.6 and 8.6 cm distance from the inlet (red band in graphs B,D). Note that for further CT analysis, these areas were ignored. Oil saturation profiles were constructed by applying a moving average (interval of 8) to the original dataset. In the bottom two cross-sectional areas are shown for 4.66 total PV injected in exp. 4 and one for the condition after slug injection in exp. 4 (E). Cross-sectional areas shown represent original CT data in Hounsfield units where the gas phase is shown in black.

injection, the shape of the formed oil bank exhibits heterogeneous characteristics where accumulation of mobilized oil happened at distinctive parts within the core (Figure 5C). The latter is the reason why two separate cross sections, that deviate from the center of the core, are shown at 0.23 PV injected. The surfactant slug clearly had a preferred area within the pore network where it mobilized S_{or_WF} (see cross-section at 5.85 cm distance from inlet in Figure 5). Most likely this is because of the core heterogeneity itself. After being mobilized at 0.23 PV, the oil tends to propagate and accumulate toward the top of the core because of a combination of core heterogeneity and gravitational forces ($\Delta\rho_{wo}$ = 0.150 ± 0.002 g/cm^3). The latter resulted in the formation of a leading edge that could spread across the entire core cross-sectional area, only at injection times later than 0.23 PV. Consistent with our earlier work, the final stationary location of the oil bank is closer to the inlet when flooding at optimum salinity compared to under-optimum salinity.[6] This might be controlled by the accessible PV for the injected slug and moveable oil and water in place, which is higher at optimum salinity conditions because of increased displacement efficiency.

The stabilities of both the displacement front at the trailing edge and leading edge (respectively interfaces 1 and 2 in Figure 5A,C) are a combined function of capillary, viscous, and gravitational forces.[44] They can be analyzed in terms of capillary number, that is, ratio of viscous forces to IFT, and bond number, that is, ratio of gravitational forces to IFT. Relatively, capillary forces are expected to have a minimal effect on the interface stability as the surfactant slug yielded an increase in capillary and bond number of a factor 1000 (under-optimum) and 10 000 (optimum) compared to water flooding (Figure 5F). As aforementioned, the relative dominance of gravitational forces increased during oil mobilization at low o/w IFT conditions, compared to water flooding, which is in good agreement with earlier work.[45] However, the either stabilizing or destabilizing effect of viscous forces on both displacement fronts can be observed. Let us define the viscosity ratio as the total viscosity upstream over the total viscosity downstream of a particular interface, such that if >1 viscous forces tend to stabilize the interface. Averaged viscosity ratios of 0.83 and 1.14 were calculated, for interfaces 1 and 2, respectively, for exp. 3. In exp. 4, these ratios equaled 0.65 (interface 1) and 1.25 (interface 2). At both salinities studied, interface 2 reveals a more stable front compared to interface 1. Note that this effect is of a higher magnitude in exp. 4 compared to exp. 3 because of sharper contrasts in viscosity ratios as a result of a more favorable displacement efficiency, that is, lower o/w IFT.

The total pressure drop profiles obtained during surfactant slug injection in exp. 3 and 4 are shown in Figure 5E. For exp. 3, a roughly constant total pressure drop can be observed. This is most likely a result of the fairly constant peak S_o within the oil bank which yielded constant averaged phase saturations and, thus, relative permeabilities. The pressure drop profile related to exp. 4 remained constant until it started to gradually increase after 0.30 ± 0.02 PV injection because of the formation of the oil bank.[21] The latter might be explained by an increase in the oil bank's peak S_o as injection continued. As peak S_o increased, local water mobility decreased which could lead to an increase in total pressure drop that was not compensated by the local increase in oil mobility.[6]

3.3.2. Oil Bank Displacement by Drive Foam. After surfactant slug injection for oil mobilization, drive foam was either generated in situ by co-injection of surfactant drive solution with N_2 (exp. 2, 3, and 4) or pregenerated ex situ and then injected in the core (exp. 5). This section presents the obtained total pressure drops and, when available, acquired CT

DOI: 10.1021/acs.energyfuels.9b00645
Energy Fuels 2019, 33, 4951−4963

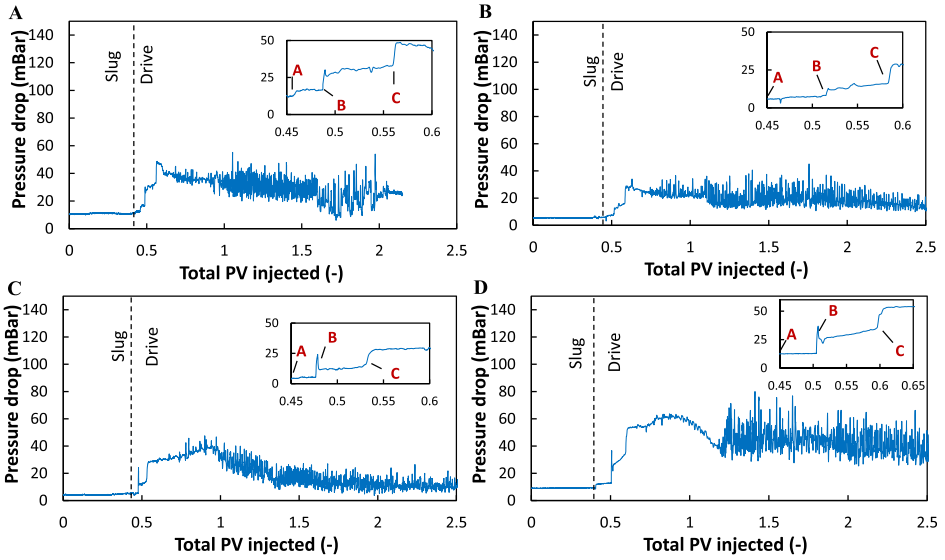

Figure 7. Total pressure drop profiles during surfactant slug and drive foam injection for exp. 2 (A), exp. 3 (B), exp. 4 (C) and exp. 5 (D). The total superficial velocity during drive foam injection equaled 2.1 ± 0.1 ft/day in all FACF core-floods. In each pressure drop plot, a second graph is presented in the top right corner that zooms in on early drive foam injection times where (A–C) refer to the times drive liquid injection started, drive N_2 injection was initiated and when both injectants entered the core, respectively. The high fluctuations in pressure drop are due to gas/foam leaving the backpressure. Presented pressure drop profiles were constructed by applying a moving average (interval of 6) to the original data. Note that PV refers to total PV, that is, slug + drive.

scan images and associated S_o profiles during drive foam injection for exp. 2, 3, 4, and 5.

Again, at first CT images and related S_o profiles for exp. 3 and 4 will be discussed as they give insight in saturation distributions which affect the measured total pressure drops. They are shown in Figure 6. Note that hereafter, PV refers to the sum of gas and liquid PV injected in slug and drive (that is, total PV). Let us first consider the presented data related to exp. 3 (Figure 6A,B). Initiating co-injection into the system led to spreading of the oil bank, that is, increasing the difference in propagation velocity between its leading and trailing edge. It caused a reduction of the oil bank's peak S_o, now only slightly higher than S_{or_WF}. Breakthrough of the oil bank happened at 0.63 ± 0.02 PV injected. Lastly, after complete production of the oil bank, a fair homogeneous residual oil saturation to FACF was achieved: S_{or_FACF} of 0.21 ± 0.03 (Figure 6B and Table 5).

The CT images for exp. 4 show the same alteration in oil bank shape because of initiation of drive co-injection: a more unstable, spread out behavior of the banked oil. Although peak S_o reduced during co-injection, it is still significantly higher than S_{or_WF}. A S_{or_FACF} of 0.16 ± 0.06 was reached at the end of the experiment (Table 5). Breakthrough of the oil bank occurred at 0.67 ± 0.02 PV injected. The nonuniform behavior of S_{or_FACF} (4.66 total PV in Figure 6C,D) is a result of dominant gravitational forces. They resulted in mainly the lower part of the core being properly swept because of the underriding tendency of the surfactant slug (Section 3.3.1). This effect is less observable in exp. 3 (Figure 6A) because of a worse displacement efficiency, that is, higher o/w IFT, compared with exp. 4. Figure 6E shows several cross-sectional areas for the scan taken at 4.66 total PV, that is, slug + drive, injected in exp. 4. A more equally divided gas phase across the entire cross-sectional area was observed downstream in the core, which is consistent with our earlier observations.[6,23] It might be a qualitative indicator of foam generation or an increasing foam strength. At locations closer to the inlet, the injected N_2 tends to partly override. Note that this feature was not observed in exp. 3.

The total pressure drops obtained during surfactant slug and drive foam injection in exp. 2, 3, 4, and 5 are presented in Figure 7. Let us first focus on the under-optimum salinity FACF core-floods: exp. 2 and 3 (Figure 7A,B). When co-injection started, and co-injected gas and liquid entered the core, a step-wise increase in pressure drop toward 46 ± 2 mbar (exp. 2) and 28 ± 2 mbar (exp. 3) was observed. This is because of the fact that the injection of the liquid drive solution started slightly earlier than N_2 injection, both at higher flow rates compared to slug injection (Table 3). This was done in order to make sure both phases entered the core simultaneously (Figure 2). Exp. 2 yielded higher pressure drops because of the lower absolute permeability of the sandstone used (Table 1). After the initial jump in pressure drop, both exp. 2 and 3 reveal a slight reduction. We propose that the moderate reduction in total pressure drop in both exp. 2 and 3 is the combined result of the reduction in the peak S_o of the oil bank, that is, increasing water mobility, and the absence of stable foam generation. Gas breakthrough occurred after 0.95 ± 0.02 and 1.11 ± 0.02 PV in exp. 2 and 3, respectively, resulting in pressure drop fluctuations as gas is leaving the backpressure. Co-injection stopped after 2.15 ± 0.02 PV injection in exp. 2 as no more oil was produced. Mobility reduction factor (MRF), which is defined as the steady-state pressure drop of drive foam injection over single-phase brine flooding at the same superficial velocity, equaled 4 ± 2 in both experiments.

The pressure drop profile for exp. 4 (Figure 7C) shows the same step-wise increase toward 28 ± 2 mbar as soon as the co-injected gas and drive fluid entered the core. Afterward, instead of a slight reduction (exp. 2 and 3), the total pressure drop started to increase gradually. The gradually increasing total pressure drop observed in exp. 4 occurred as soon as the co-injectants reached the oil bank. This is in good agreement with our earlier work at model conditions.[23] This may be explained

DOI: 10.1021/acs.energyfuels.9b00645
Energy Fuels 2019, 33, 4951–4963

as follows. A rather weak drive foam was generated and propagated upstream of the oil bank. However, foam generation seems to increase upon touching the oil bank, yielding the more equally divided gas phase (Figure 6E), thus displacing the banked oil toward the outlet. The proposed mechanism for the latter includes a reduction in effective porosity once the drive foam reached the banked oil, an increment in gas and liquid interstitial velocities and subsequently an increasing local pressure drop which might promote foam generation.[23,46] After foam breakthrough (at 0.99 ± 0.02 PV), total pressure drop decreased toward a steady-state value corresponding to a MRF of 4 ± 2. Comparison with exp. 3 (under-optimum salinity) indicates that a somewhat more favorable, that is, lower, drive mobility was achieved in exp. 4 (optimum salinity) during oil bank displacement.

For assessing the impact of pregenerated foam on the measured total pressure drops during drive foam injection, exp. 4 is compared with exp. 5 (Figure 7C,D). Directly, after the pregenerated foam entered the sandstone core, an instantaneous jump in pressure drop to 53 ± 1 mbar was seen. Subsequently, a small increase followed by a gradually decreasing trend in pressure difference was measured. This behavior is most probably related to a combination of the oil bank being produced and further development of the drive foam. Eventually, after breakthrough of the drive foam at 1.24 ± 0.02 PV, pressure drops reached steady values in agreement with an averaged MRF of 9 ± 3. Results showed that injecting a pregenerated foam drive (exp. 5) yields a more favorable drive mobility, delayed foam breakthrough, and thus a more efficient displacement of the banked oil compared to in situ drive foam generation (exp. 4).

3.3.3. Oil Recovery. Figure 8 presents the cumulative oil recovery profiles during water flooding (exp. 5) and surfactant slug and drive co-injection (exp. 3, 4, and 5). The recovery profiles for exp. 2 could not be generated because of electrical failures. Because all FACF core-floods performed showed very similar oil recovery profiles during water flooding, only exp. 5 is highlighted here. Prior to water breakthrough, an oil recovery of 48 ± 3% of the oil initially in place (OIIP) was reached.

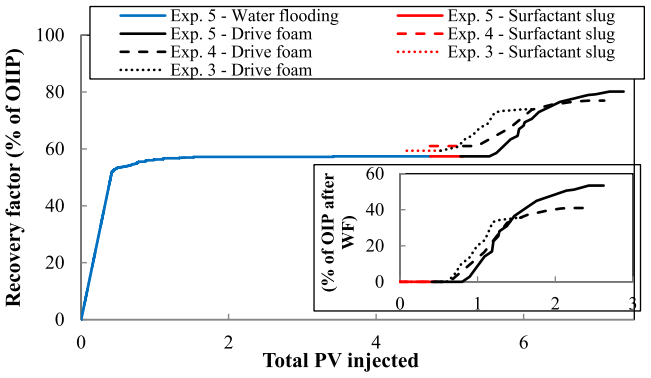

Figure 8. Oil recovery profiles during water flooding (exp. 5), surfactant slug, and drive foam injection (exp. 3, 4, and 5). The recovery shown is expressed as a percentage of the OIIP. The lower right graph states the oil recovery, during surfactant slug and drive injection in exp. 3, 4, and 5, as percentage of the OIP after water flooding. All recovery profiles were constructed using material balance calculations. Drive injection continued in each experiment until no more oil was produced.

This could be increased further to 58 ± 3% of the OIIP at the end of water flooding (Table 5). In the next sections, the effects of slug salinity and drive foam strength, that is, co-injection versus pregenerated, on the oil recovery during the performed FACF core-foods will be discussed.

For assessing the impact of surfactant slug salinity, exp. 3 (under-optimum salinity) is compared with exp. 4 (optimum salinity). When shifting from under-optimum salinity conditions in exp. 3 toward the optimum salinity applied in exp. 4, the recovery factor could be increased with 5% of the OIP after water flooding. This can be attributed to a better displacement efficiency, that is, lower o/w IFT, in exp. 4. Moreover, the pressure drop profile related to exp. 4 (Figure 7C) also suggest a more favorable, lower, drive mobility during oil bank displacement (compared with exp. 3) which may promote oil recovery in exp. 4. Oil bank breakthrough happened slightly earlier in exp. 3 compared to exp. 4 because of the oil bank shape and position, formed during slug injection (Figures 5A vs 4C). After complete production of the banked oil in exp. 3 and 4, part of the oil was produced as solubilized oil, resulting in the tail-shaped production profile after approximately 1.30 ± 0.20 total PV slug and drive injected (Figure 8). Note that this effect is more pronounced in exp. 4 because of the presence of a type III distinct ME that exhibits a higher oil fraction (~0.8) than a type II(−) ME (~0.1) (exp. 3).

For studying the impact of drive foam strength (pregenerated vs in situ generated) on the oil being recovered in a FACF process conducted at optimum salinity, exp. 4 is compared with exp. 5. The experimental results presented in this work showed that the ultimate oil recovery could be increased with 13% of the OIP after water flooding when injecting pregenerated drive foam as an alternative to conducting co-injection. The increment in oil recovery can be fully assigned to the more favorable drive mobility, that is, higher apparent drive foam viscosity, in exp. 5 as the o/w IFT and total injection rates were kept constant. The more promising drive mobility in exp. 5 most probably also resulted in a somewhat more efficient oil bank displacement which in turn might explain the delayed oil bank breakthrough time compared to exp. 4. In exp. 4, the gravity underriding tendency of the liquid slug and drive (Figures 5C and 6C) might yield a relatively early breakthrough of the oil bank's leading edge. After approximately 2.05 ± 0.02 PV slug and drive injected a type III ME broke through in exp. 5.

4. GENERAL DISCUSSION

In this section, the results presented and observations made in this paper will be discussed in terms of applicability to real-field conditions. Our experimental setting yielded a capillary number (formula in caption of Figure 5) of 10^{-5} and 10^{-4} for under-optimum and optimum salinity conditions, respectively. It resulted in the mobilization of S_{or_WF} as depicted in Figure 5. One may argue whether it is realistic to expect the same relative amount of oil being mobilized at the conditions of the case study reservoir, at constant capillary number. This is most likely not the case. Although reservoir rocks exhibit similar porosities compared to the Bentheimer sandstone cores used in this work (Section 2.2), their absolute permeability is significantly lower (0.64 D vs 3.39 ± 0.47 D). At fixed capillary number, that is, constant injection velocity, o/w IFT and fluid viscosity, a lower absolute permeability will result in a higher pressure drop. The latter implying an increased capacity to mobilize and displace residual oil, during surfactant slug

DOI: 10.1021/acs.energyfuels.9b00645
Energy Fuels 2019, 33, 4951−4963

injection, at the conditions of the case study reservoir compared to the experimental setting in this work.[47] Note that the latter is only valid when we assume a similar, unaltered, rock wettability for the reservoir rock compared to the cores used in this work. However, because reservoir pressures are in the order of 200 bar, which is far higher than the experimental pressure of 20 bar, this assumption might be too simplistic. As elevated pressures may cause the reservoir rock to change its wettability toward more oil-wet conditions,[48] oil may be absorbed onto the rock which subsequently can lead to a higher capillary resistance that enhances the pressure drop. In this case, higher pressure drop does not necessarily imply larger mobilization capacity of residual oil.

As discussed in Sections 3.3.1 and 3.3.2, the relatively dominant gravitational forces led to an unstable oil bank formation at both slug salinities studied in this work (Figure 5). It is essential to note that these observations are related to a sandstone core with a diameter of 3.80 ± 0.10 cm only. The case study reservoir has an averaged net thickness of approximately 18 m. It is expected that for real field conditions, the gravity underriding effect of the liquid surfactant slug is of a considerably higher magnitude compared to the experimental findings in this work. As a consequence, most probably only the lower part of the reservoir will be properly swept (Figure 6C). One might compensate for this effect by adding a polymer to or foam the surfactant slug in order to favor the mobility ratio.[49]

The core-flood experiments conducted in this study showed that injection of pregenerated Surfactant X drive foam yielded an increase of 13% of the OIP after water flooding compared to in situ drive foam generation at optimum salinity (exp. 4 vs exp. 5) because of the more favorable drive mobility. In terms of real field conditions, exp. 5 might be quite representative. Assuming near-zero oil saturations in the near-wellbore region, as a consequence of the relatively high pressure drop in that area, it might function as a foam generator (equivalent to the mixing tee installed for exp. 5 (Figure 2)).

5. CONCLUSIONS

A laboratory study on the feasibility of FACF for EOR was conducted at reservoir temperature of 90 ± 1 °C in Bentheimer sandstones utilizing crude oil. Dedicated phase behavior and bulk foam experiments yielded the design of a surfactant slug and drive solution that was used in core-flood experiments. Controlled (CT-assisted) FACF core-flood experiments were performed where an IOS2024 surfactant slug mobilized residual oil to waterflood and, afterward, Surfactant X drive foam displaced the mobilized oil bank. Drive foam strength, that is, in situ drive foam generation by co-injection versus injecting a pregenerated drive foam, and surfactant slug salinity were varied. This study resulted in the following main conclusions:

- Phase behavior studies performed at reservoir temperature showed that Surfactant X does not lower the oil-water IFT to ultralow values, whereas IOS2024 does. The designed IOS2024 surfactant slug revealed a Winsor type III system (optimum salinity conditions) at salinities of 1.50−1.75 wt % NaCl + KCl. The addition of 1-iododecane to the oleic phase did not alter the crude oil-IOS2024 phase behavior.
- Bulk foam experiments in the absence of oil showed a roughly 11 times greater foam half-decay time for the Surfactant X drive solution compared to the IOS2024 drive formulation. The addition of 5 volume percent crude oil to the drive solution reduced the foam half-decay time of the Surfactant X drive foam with approximately a factor 12 in bulk.
- The foam quality scan showed that the Surfactant X drive formulation was able to generate strong, stable foams in a Bentheimer sandstone for all gas fractional flows assessed in the absence of crude oil. The largest apparent foam viscosity of 1.45 ± 0.11 Pa·s was reached at a foam quality of 75.0%. Foam qualities below are in the low foam-quality regime, whereas higher foam qualities describe the high-quality regime. A 57.5% foam quality resulted in an apparent foam viscosity of 1.32 ± 0.05 Pa·s.
- An unstable oil bank was formed during both under-optimum and optimum salinity FACF because of relatively dominant gravitational forces. The IOS2024 surfactant slug at optimum salinity was significantly more effective at reducing residual oil to waterflood (81% reduction) compared to the under-optimum salinity slug (30% reduction).
- Optimum salinity FACF was able to increase its ultimate oil recovery to 40 ± 5% of the OIP after water flooding while under-optimum salinity FACF yielded an oil recovery of 35 ± 7%. The injection of pregenerated Surfactant X drive foam yielded an increase of 13% of the OIP after water flooding compared to in situ drive foam generation by co-injection, both performed at optimum salinity.

■ ASSOCIATED CONTENT

Supporting Information

The Supporting Information is available free of charge on the ACS Publications website at DOI: 10.1021/acs.energyfuels.9b00645.

Properties of the used chemicals, physical properties of all liquid phases used in the core-flood experiments, and densities and viscosities measured at 90 ± 1 °C (PDF)

■ AUTHOR INFORMATION

Corresponding Author

*E-mail: mjanssen2@outlook.com.

ORCID

Martijn T. G. Janssen: 0000-0002-0940-4998

Rashidah M. Pilus: 0000-0001-5720-3923

Notes

The authors declare no competing financial interest.

■ ACKNOWLEDGMENTS

This study is the result of a collaboration between Delft University of Technology, Universiti Teknologi Petronas, Petronas and Shell. We are grateful to Petronas and Shell for funding the project. The authors thank Shell and Petronas for the supply of materials and data. Michiel Slob (TU Delft), Ellen Meijvogel-de Koning (TU Delft) and Jens van den Berg (TU Delft) are gratefully acknowledged for their technical support.

DOI: 10.1021/acs.energyfuels.9b00645
Energy Fuels 2019, 33, 4951−4963

REFERENCES

(1) Zhu, T.; Ogbe, D. O.; Khataniar, S. Improving the foam performance for mobility control and improved sweep efficiency in gas flooding. *Ind. Eng. Chem. Res.* **2004**, *43*, 4413−4421.

(2) Rossen, W. R.; Van Duijn, C. J.; Nguyen, Q. P.; Vikingstad, A. K. *Injection Strategies to Overcome Gravity Segregation in Simultaneous Gas and Liquid Injection into Homogeneous Reservoirs*; Society of Petroleum Engineers, 2006.

(3) Farajzadeh, R.; Andrianov, A.; Bruining, H.; Zitha, P. L. J. Comparative Study of CO2and N2Foams in Porous Media at Low and High Pressure−Temperatures. *Ind. Eng. Chem. Res.* **2009**, *48*, 4542−4552.

(4) Bhoendie, K. S.; Moe Soe Let, K. P.; Li, T.; Zitha, P. L. J. *Laboratory Evaluation of Gas-Injection EOR for the Heavy-Oil Reservoirs in Suriname*; Society of Petroleum Engineers, 2014.

(5) Talebian, S. H.; Masoudi, R.; Tan, Isa Mohd.; Zitha, P. L. J. Foam assisted CO2-EOR: A review of concept, challenges, and future prospects. *J. Pet. Sci. Eng.* **2014**, *120*, 202−215.

(6) Janssen, M. T. G.; Pilus, R. M.; Zitha, P. L. J. A Comparative Study of Gas Flooding and Foam-Assisted Chemical Flooding in Bentheimer Sandstones. *Transp. Porous Media* **2019**, DOI: 10.1007/s11242-018-01225-3.

(7) Andrianov, A. I.; Liu, M. K.; Rossen, W. R. *Sweep Efficiency in CO_2 Foams Simulations with Oil*; Society of Petroleum Engineers, 2011.

(8) Kovscek, A. R.; Radke, C. J. Fundamentals of foam transport in porous media. *Foams: Fundamentals and Applications in the Petroleum Industry*; American Chemical Society, 1994; pp 115−163.

(9) Rossen, W. R. Foams in Enhanced Oil Recovery. In *Foams: Theory Measurements and Applications*; Prud'homme, R. K., Khan, S., Eds.; Marcel Dekker: New York City, 1996.

(10) Zitha, P. L. J.; Nguyen, Q. P.; Currie, P. K.; Buijse, M. A. Coupling of foam drainage and viscous fingering in porous media revealed by X-ray computed tomography. *Transp. Porous Media* **2006**, *64*, 301−313.

(11) Du, D.; Zitha, P. L. J.; Uijttenhout, M. G. H. Carbon dioxide foam rheology in porous media: a CT scan study. *SPE J.* **2007**, *12*, 245−252.

(12) Zitha, P. L. J.; Du, D. X. A new stochastic bubble population model for foam flow in porous media. *Transp. Porous Media* **2010**, *83*, 603−621.

(13) Simjoo, M.; Dong, Y.; Andrianov, A.; Talanana, M.; Zitha, P. L. J. CT scan study of immiscible foam flow in porous media for enhancing oil recovery. *Ind. Eng. Chem. Res.* **2013**, *52*, 6221−6233.

(14) Lake, L. W. *Enhanced Oil Recovery*; Prentice-Hall: Englewood Cliffs, New Jersey, 1989.

(15) Aronson, A.S.; Bergeron, V.; Fagan, M.E.; Radke, C.J. The influence of disjoining pressure on foam stability and flow in porous media. *Colloids Surf., A* **1994**, *83*, 109−120.

(16) Howe, A. M.; Clarke, A.; Mitchell, J.; Staniland, J.; Hawkes, L. A. *Visualising Surfactant EOR in Core Plugs and Micromodels*; Society of Petroleum Engineers, 2015.

(17) Yang, Y.; Yang, H.; Tao, L.; Yao, J.; Wang, W.; Zhang, K.; Luquot, L. Microscopic Determination of Remaining Oil Distribution in Sandstones With Different Permeability Scales Using Computed Tomography Scanning. *J. Energy Resour. Technol.* **2019**, *141*, 092903.

(18) Hou, B.-f.; Wang, Y.-f.; Huang, Y. Mechanistic study of wettability alteration of oil-wet sandstone surface using different surfactants. *Appl. Surf. Sci.* **2015**, *330*, 56−64.

(19) Wang, Y.; Xu, H.; Yu, W.; Bai, B.; Song, X.; Zhang, J. Surfactant induced reservoir wettability alteration: Recent theoretical and experimental advances in enhanced oil recovery. *Pet. Sci.* **2011**, *8*, 463−476.

(20) Hirasaki, G. J.; Miller, C. A.; Puerto, M.. *Recent advances in surfactant EOR*; SPE Annual Technical Conference and Exhibition, 2011; Vol. *16* (4), pp 889−907.

(21) Guo, H.; Zitha, P. L. J.; Faber, R.; Buijse, M. A novel alkaline/surfactant/foam enhanced oil recovery process. *SPE J.* **2012**, *17*, 1186−1195.

(22) Jong, S.; Nguyen, N. M.; Eberle, C. M.; Nghiem, L. X.; Nguyen, Q. P. *Low Tension Gas Flooding as a Novel EOR Method: An Experimental and Theoretical Investigation*; Society of Petroleum Engineers, 2016.

(23) Janssen, M. T. G.; Zitha, P. L. J.; Pilus, R. M. *Oil Recovery by Alkaline-Surfactant-Foam (ASF) Flooding: Effect of Drive Foam Quality on Oil Bank Propagation*; Society of Petroleum Engineers, 2018.

(24) Hu, Y.; Devegowda, D.; Striolo, A.; Phan, A.; Ho, T. A.; Civan, F.; Sigal, R. F. Microscopic dynamics of water and hydrocarbon in shale-kerogen pores of potentially mixed wettability. *SPE J.* **2014**, *20*, 112−124.

(25) Liang, L.; Luo, D.; Liu, X.; Xiong, J. Experimental study on the wettability and adsorption characteristics of Longmaxi Formation shale in the Sichuan Basin, China. *J. Nat. Gas Sci. Eng.* **2016**, *33*, 1107−1118.

(26) Pan, B.; Jones, F.; Huang, Z.; Yang, Y.; Li, Y.; Hejazi, S. H.; Iglauer, S. Methane (CH4) wettability of clay coated quartz at reservoir conditions. *Energy Fuels* **2019**, *33*, 788.

(27) Winsor, P. A. *Solvent Properties of Amphiphilic Compounds*; Butterworths Scientific Publications. Ltd.: London, 1954.

(28) Hosseini-Nasab, S. H.; Zitha, P. L. J. Systematic phase behaviour study and foam stability analysis for optimal alkaline/surfactant/foam enhanced oil recovery. *IOR 2015-18th European Symposium on Improved Oil Recovery*, 2015.

(29) Chatterjee, J.; Wasan, D. T. A kinetic model for dynamic interfacial tension variation in an acidic oil/alkali/surfactant system. *Chem. Eng. Sci.* **1998**, *53*, 2711−2725.

(30) Nešić, S. Key issues related to modelling of internal corrosion of oil and gas pipelines−A review. *Corros. Sci.* **2007**, *49*, 4308−4338.

(31) Srivastava, M.; Zhang, J.; Nguyen, Q. P.; Pope, G. A. A Systematic Study of Alkali Surfactant Gas Injection as an Enhanced Oil Recovery Technique. *SPE Annual Technical Conference and Exhibition*; Society of Petroleum Engineers, 2009.

(32) Peksa, A. E.; Wolf, K.-H. A. A.; Zitha, P. L. J. Bentheimer Sandstone Revisited for Experimental Purposes. *Mar. Pet. Geol.* **2015**, *67*, 701−719.

(33) Skauge, A.; Fotland, P. Effect of pressure and temperature on the phase behavior of microemulsions. *SPE Reservoir Eng.* **1990**, *5*, 601−608.

(34) Kapetas, L.; Vincent Bonnieu, S.; Danelis, S.; Rossen, W. R.; Farajzadeh, R.; Eftekhari, A. A.; Mohd Shafian, S. R.; Kamarul Bahrim, R. Z. *Effect of Temperature on Foam Flow in Porous Media*; Society of Petroleum Engineers, 2015.

(35) Darcy, H. *Les fontaines publiques de la ville de Dijon: exposition et application*; Victor Dalmont, 1856.

(36) Sheng, J. *Modern Chemical Enhanced Oil Recovery: Theory and Practice*; Gulf Professional Publishing, 2010.

(37) Osterloh, W. T.; Jante, M. J. *Effects of Gas and Liquid Velocity on Steady-State Foam Flow at High Temperature*; Society of Petroleum Engineers, 1992.

(38) Alvarez, J. M.; Rivas, H. J.; Rossen, W. R. Unified Model for Steady-State Foam Behavior at High and Low Foam Qualities. *SPE J.* **2001**, *6*, 325−333.

(39) Jones, S.A.; Van Der Bent, V.; Farajzadeh, R.; Rossen, W.R.; Vincent-Bonnieu, S. Surfactant screening for foam EOR: Correlation between bulk and core-flood experiments. *Colloids Surf., A* **2016**, *500*, 166−176.

(40) Aarra, M. G.; Skauge, A. *A Foam Pilot in a North Sea Oil Reservoir: Preparation for a Production Well Treatment*; Society of Petroleum Engineers, 1994.

(41) Tang, J.; Bonnieu, S. V.; Rossen, W. R. The Effect of Oil on Steady-state Foam Flow Regimes in Porous Media. *IOR 2017-19th European Symposium on Improved Oil Recovery*, 2017.

(42) Simjoo, M.; Rezaei, T.; Andrianov, A.; Zitha, P.L.J. Foam stability in the presence of oil: effect of surfactant concentration and oil type. *Colloids Surf., A* **2013**, *438*, 148−158.

(43) Osei-Bonsu, K.; Shokri, N.; Grassia, P. Foam stability in the presence and absence of hydrocarbons: From bubble- to bulk-scale. *Colloids Surf., A* **2015**, *481*, 514−526.

DOI: 10.1021/acs.energyfuels.9b00645
Energy Fuels 2019, 33, 4951−4963

(44) Lovoll, G.; Méheust, Y.; Måløy, K. J.; Aker, E.; Schmittbuhl, J. Competition of gravity, capillary and viscous forces during drainage in a two-dimensional porous medium, a pore scale study. *Energy* **2005**, *30*, 861−872.
(45) Oughanem, R.; Youssef, S.; Bazin, B.; Maire, E.; Vizika, O. Pore-scale to core-scale aspects of capillary desaturation curves using CT-scan imaging. *IOR 2013-17th European Symposium on Improved Oil Recovery*, 2013.
(46) Rossen, W. R.; Gauglitz, P. A. Percolation Theory of Creation and Mobilization of Foams in Porous Media. *AIChE J.* **1990**, *36*, 1176−1188.
(47) Yeganeh, M.; Hegner, J.; Lewandownski, E.; Mohan, A.; Lake, L. W.; Cherney, D.; Jusufi, A.; Jaishankar, A. *Capillary Desaturation Curve Fundamentals*; Society of Petroleum Engineers, 2016.
(48) Pan, B.; Li, Y.; Wang, H.; Jones, F.; Iglauer, S. CO2 and CH4 Wettabilities of Organic-Rich Shale. *Energy Fuels* **2018**, *32*, 1914−1922.
(49) Turta, A. Enhanced Oil Recovery Field Case Studies. *In Situ Combustion*; Elsevier Inc. Chapters, 2013; Chapter 18.

DOI: 10.1021/acs.energyfuels.9b00645
Energy Fuels 2019, 33, 4951−4963